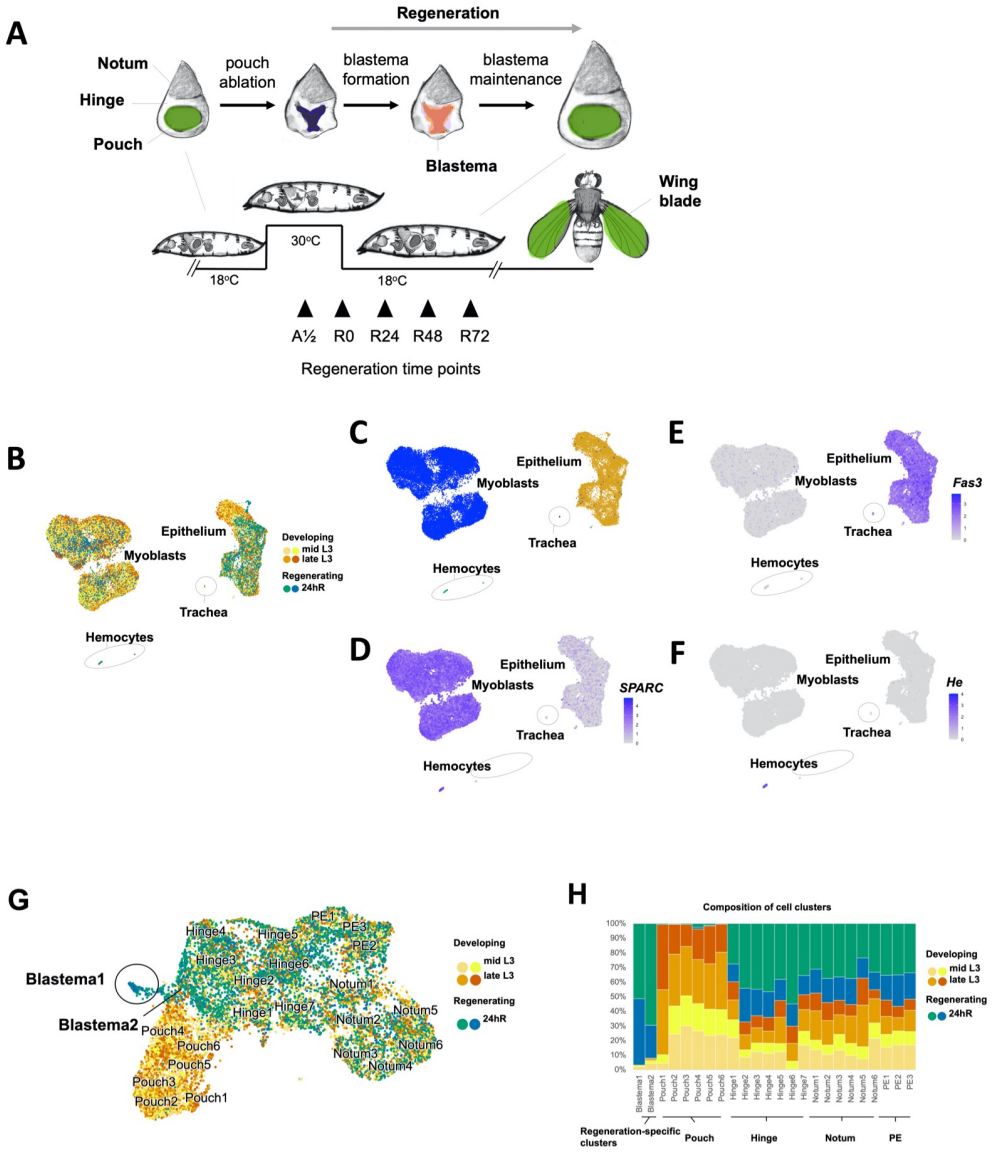

Figure S1. Single-cell analysis of regenerating wing imaginal discs. Related to Figure 1. (**A**) Schematic of genetic ablation system. The canonical domains of the wing disc and the adult structures to which they give rise are colored in gray (notum), white (hinge), and green (pouch). The wing pouch gives rise to the adult wing blade. Expression of the pro-apoptotic gene *eiger* is targeted to the wing pouch using *rn-GAL4* and *UAS-eiger*. Gal4 function is inhibited at 18º C and permitted at 30º C for 40 h by inactivation of a ubiquitously-expressed temperature-sensitive Gal80 (*tub-Gal80^{ts}*). Regeneration proceeds after the formation of the blastema (orange). R0, R24, R48, and R72 indicate the number of hours after the onset of regeneration following the downshift to 18º C. A1/2 indicates the midpoint of the ablation phase. (**B**) Harmonized UMAP of scRNAseq data from developing and regenerating wing imaginal discs. Data colored by sample of origin and major cell types are annotated. Samples were derived from developing discs at the middle and late stages of the third larval instar (L3), as described previously [S1], and from regenerating discs 24 h after the downshift to 18º C (R24). Two biological replicates were obtained for each sample (see Materials and Methods). The three major cell types identified were epithelial cells, myoblasts, and hemocytes. In addition, a few tracheal cells were also identified. The cell counts from the regenerating discs were: 6,613 epithelial cells, 7,466 myoblasts, 224 hemocytes, and 17 tracheal cells. (**C**) UMAP colored by major cell types: myoblasts, epithelial cells, and hemocytes are shown in different colors (**D-F**) Expression of marker genes for the three major cell types: (**D**) *Secreted protein, acidic, cysteine-rich* (*SPARC)* expression marks the myoblasts; (**E**) *Fasciclin 3* (*Fas3)* expression marks the epithelium; and (**F**) *Hemese* (*He)* marks the hemocytes. (**G**) UMAP of harmonized data from epithelial cells from regenerating and developing (from two time points) samples. Each dataset, including replicates, is represented in a distinct color. (**H**) Composition of cell clusters, as shown in **Figure 1B**. Note the underrepresentation of cells assigned to pouch clusters in regenerating discs and the near absence of cells assigned to the Blastema1 and Blastema2 clusters in developing discs. PE refers to the peripodial epithelium.

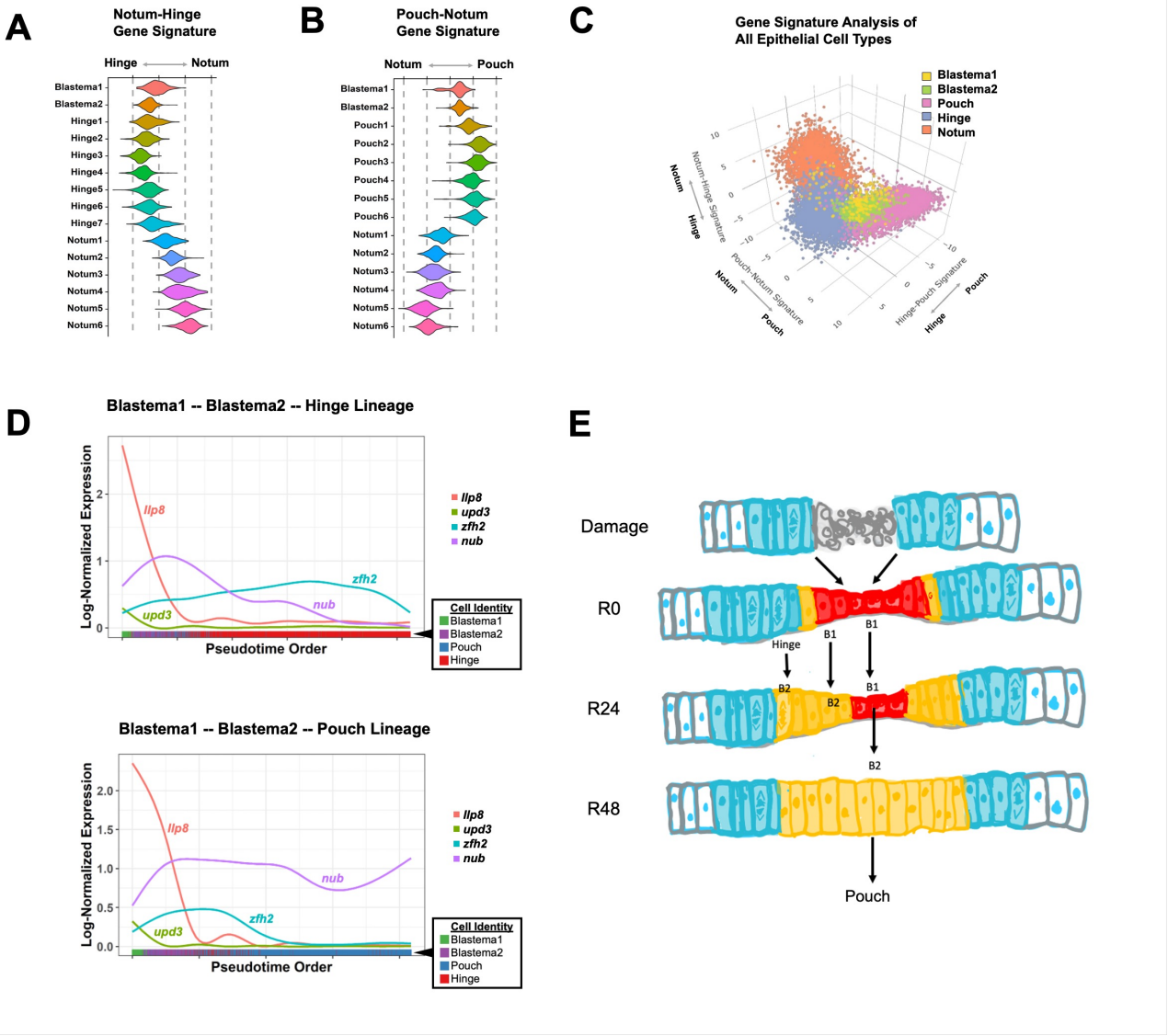

Figure S2. Gene signature and pseudotime analysis of blastema cells. Related to Figure 2. (**A-C**) Comparative gene signature analysis of major epithelial domains for the blastema clusters. (**A, B**) Clusters within the scRNAseq dataset scored with a notum-hinge (**A**) or pouch-notum (**B**) gene signature. Note that scores for the blastema clusters are more closely aligned with the hinge (**A**) or pouch (**B**) rather than the notum. The hinge-pouch signature is shown in **Figure 2I.** (**L**) 3D signature plot of scRNAseq clusters scored by notum-hinge, pouch-notum, and pouch-hinge gene signatures (axes values represent relative signature scores; see Material and Methods). Note that both Blastema1 and Blastema2 cells are primarily centered between hinge and pouch fates. (**D**) Slingshot lineage analysis of single-cell data identifies two predominant pseudotime trajectories (predicted lineages) from Blastema1 to either the Hinge or the Pouch. Note that both predicted lineages transition through Blastema2. (**E**) Model or Blastema1 and Blastema2 cell fates during regeneration depicting: (1) Blastema1 cell fate is transitory and some of these cells contribute to the regenerate (**Figure 2A-D, 2O**), (2) Blastema2 cells are recruited from Hinge cells (**Figure 2E-H**), and (3) Blastema1 cells are predicted to transition through a Blastema2 state (**Figure S2D**).

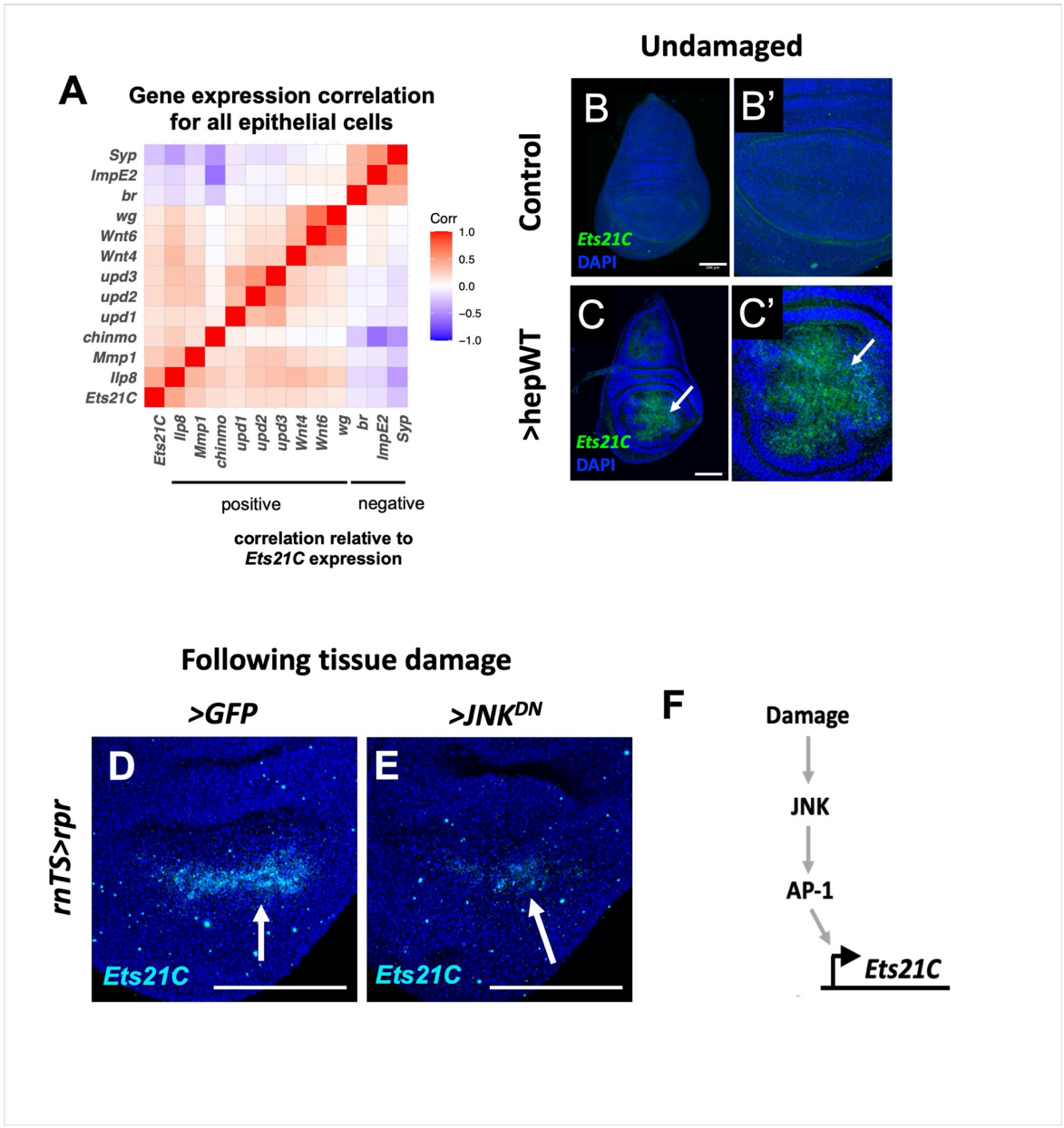

Figure S3. *Ets21C*-expression correlation during regeneration and upstream regulation of *Ets21C*. Related to Figure 3. (**A**) Genes that positively or negatively correlate with *Ets21C* expression. Pearson correlation was calculated using the normalized gene expression data within all epithelial cells (both developing and regenerating datasets). The gene with the most correlated expression to *Ets21C* expression is *Ilp8. Ets21C* expression is also positively correlated with the expression of *Mmp1, chinmo, upd1, upd2, upd3, Wnt4, Wnt6,* and *wg.* Examples of genes that show negative gene expression correlated with *Ets21C* include *broad (br), Ecdysone-inducible gene E2* (*ImpE2)*, and *Syncrip* (*Syp).* (**B, C**) Expression of *Ets21C-GFP* in a wing disc with *rn-GAL4* driving the expression of (**B**) *UAS-RFP* or (**C**) *UAS-hep*^{wt}. Note that driving the expression of the wild-type version of the JNK-kinase *hemipterous* (*hep*) within the wing pouch leads to the expression of *Ets21C-GFP.* (**D, E**) Expression of *Ets21C* following genetic ablation using *rn-Gal4*, *tub-Gal80*^{ts} and *UAS-reaper* (*rn*^{TS}*>rpr)* in the pouch while simultaneously driving *UAS-GFP* (control) or *UAS-JNK*^{DN}. Note the reduction in *Ets21C* expression when JNK signaling is blocked. (**F**) Model of upstream regulation of *Ets21C.* Microscopy scale bars = 100 μm.

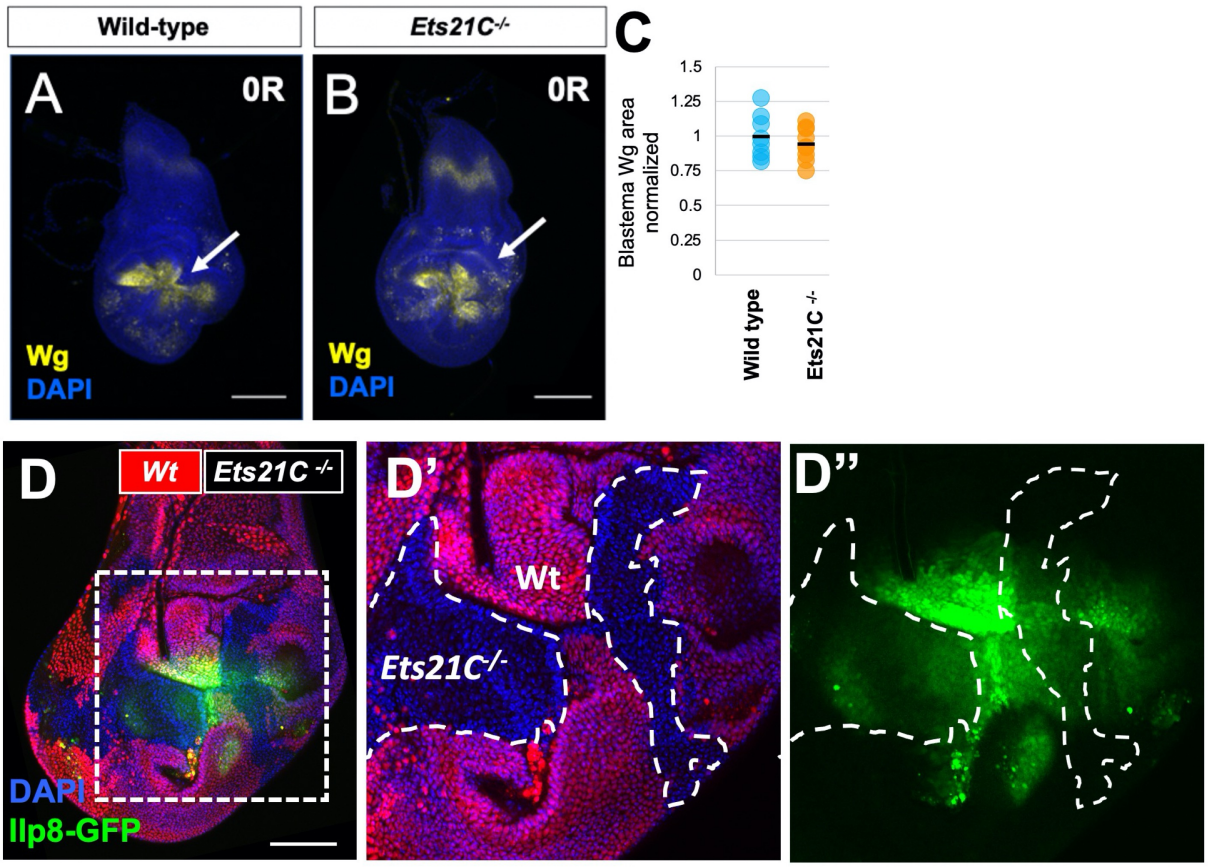

Figure S4. *Ets21C*$^{-/-}$ impact on gene expression during regeneration. Related to Figure 4. (**A-C**) Wingless (Wg) expression is still upregulated in the blastema during regeneration in *Ets21C*$^{-/-}$ mutants at comparable levels to wild-type discs. Arrows point to the region of Wg expression. (**D**) Mosaic tissues created by mitotic recombination, with *Ets21C*$^{-/-}$ mutant clones marked by the absence of RFP. Clone boundaries (arrowed) are indicated by dashed lines. Note that *Ets21C*$^{-/-}$ mutant cells are able to proliferate during regeneration, but show a cell-autonomous decrease in *Ilp8-GFP* expression after 48 h of regeneration. Note that *Ilp8-GFP* is dimmer in *Ets21C*$^{-/-}$ mutant cells (RFP-) than adjacent wild type cells (RFP+). Microscopy scale bars = 100 µm.

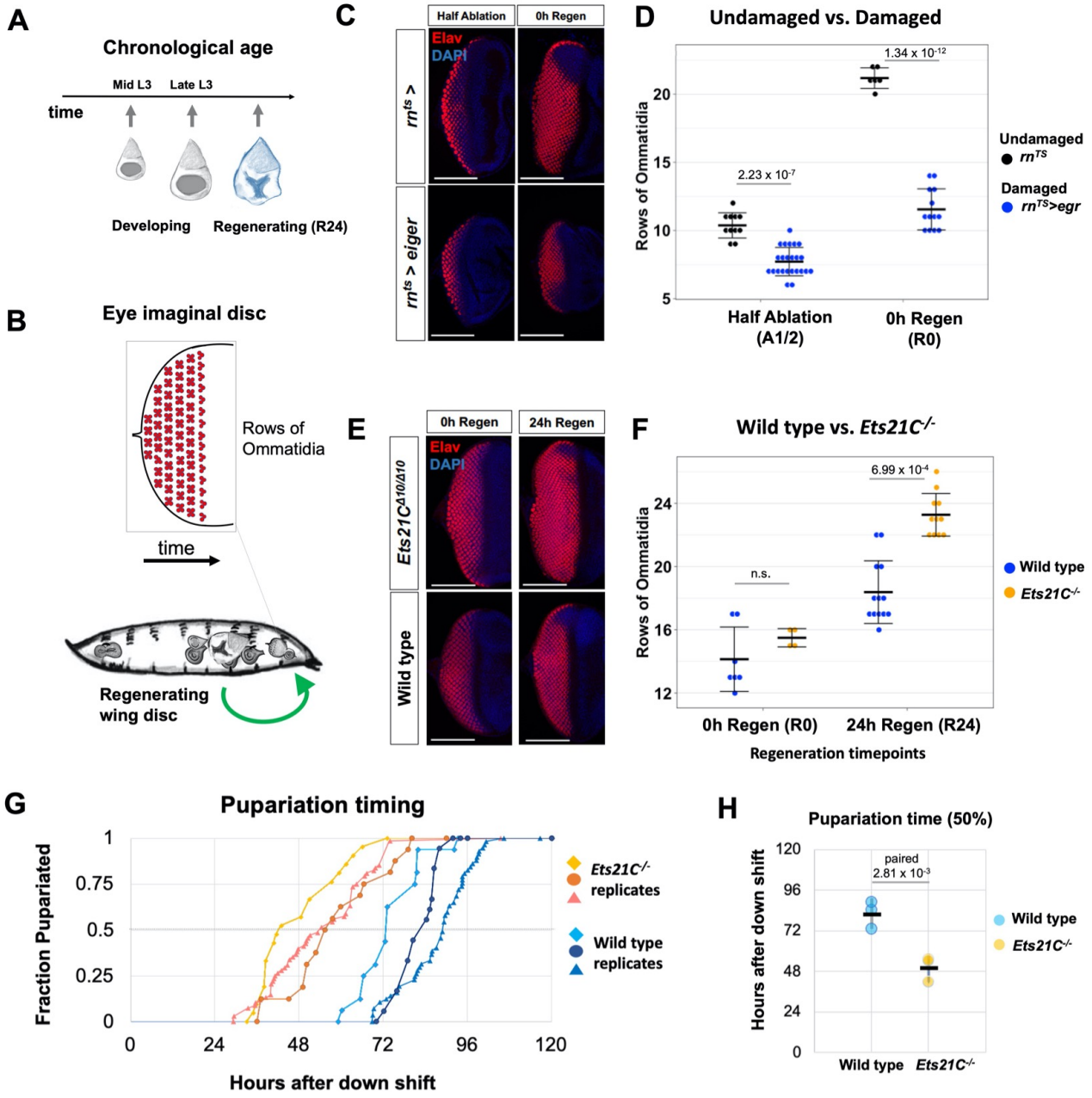

Figure S5. *Ets21C*$^{-/-}$ impact on developmental progression during regeneration. Related to Figure 5. (**A**) Diagram of the relative chronological age of our single-cell datasets. Note that the regenerating imaginal discs are chronologically older than both developmental time points, which are from mid and late 3rd instar, because tissue damage results in an extended larval phase during which regeneration occurs. (**B-F**) To investigate the developmental progression of other tissues while the wing discs are undergoing regeneration, we have counted the number of ommatidial rows within the eye-imaginal disc. (**B**) Diagram of how the "eye-clock" can be used to assess organismal-wide developmental progression. (**C, D**) The number of ommatidial rows for undamaged controls as compared to regenerating larvae. Note that the rate of addition of new rows of ommatidia added has slowed in the regenerating sample. (**E, F**) Comparison of the number of ommatidial rows for wild-type and *Ets21C*$^{-/-}$ mutants during regeneration. Note that the *Ets21C*$^{-/-}$ mutant animals show an increased number of ommatidial rows by 24h of regeneration, indicating that there is a reduction in the organism-wide developmental delay that is observed in wild-type regenerating larvae. (**G, H**) Pupariation timing for wild type and *Ets21C*$^{-/-}$ mutant animals following damage and regeneration. Replicates were conducted on separate days. (**H**) The pupariation timing was calculated based on the point when 50% of the animals had pupariated. Following ablation and regeneration, *Ets21C*$^{-/-}$ mutant larvae pupariated an average of 31 h earlier than the wild type controls. Microscopy scale bars = 100 μm.

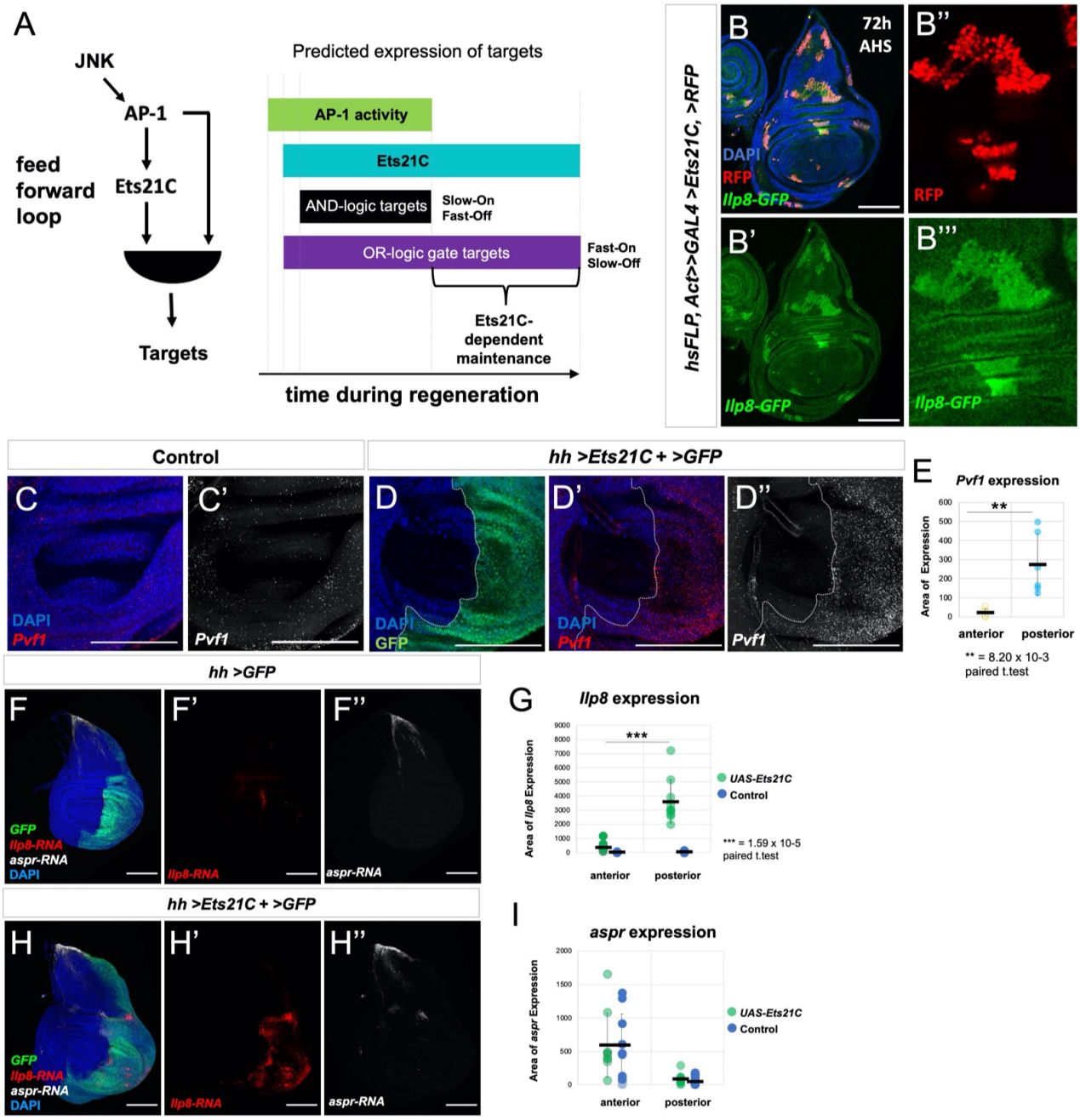

Figure S6. Gene regulatory network activated by Ets21C. Related to Figure 6. (**A**) Proposed feed forward loop with *Ets21C* and the JNK/AP1 pathway. Predicted expression dynamics of downstream target genes of AP1 and *Ets21C* depending on whether the target gene is dependent on both ("AND-Gate") or either ("OR-Gate") for expression. "AND" logic gates are predicted to turn on slow and off fast while "OR" logic gates would turn on fast and off slowly (shown in purple). (**B**) Clones of cells that overexpress *Ets21C* (marked by RFP) with the GAL4/UAS system. Note that clones of cells overexpressing *Ets21C* turn on the expression of *Ilp8-GFP*. (**C-D**) HCR for *Pvf1* in (**C**) control and (**D**) *Ets21C*-overexpressing discs. *UAS-Ets21C* is overexpressed in the posterior compartment of the disc using *hedgehog-GAL4 (hh-Gal4)* (marked by UAS-GFP). (**E**) Quantification of *Pvf1* area of expression between anterior and posterior sides of the wing discs (this analysis focused on the wing pouch region and excluded both the notum and PE that have some endogenous *Pvf1* expression). Note that *UAS-Ets21C* expression significantly increases the levels of *Pvf1*. (**F-I**) Overexpression of GFP alone (**F**) or together with *Ets21C* (**H**) in the posterior compartment of undamaged wing imaginal discs. HCR for *Ilp8-RNA* and *aspr-RNA* in marked channels. Note that *Ilp8-RNA* is expressed at significantly higher levels in the posterior when *UAS-Ets21C* was expressed. (**G, I**) Images were quantified by comparing the expression in anterior (control) and posterior (UAS-expressing) compartments. *aspr-RNA* is normally detected in the anterior notum region and no significant change was detected when *Ets21C* was expressed. Microscopy scale bars = 100 μm.

Supplemental Reference:

S1 Everetts, N.J., Worley, M.I., Yasutomi, R., Yosef, N., and Hariharan, I.K. (2021). Single-cell transcriptomics of the Drosophila wing disc reveals instructive epithelium-to-myoblast interactions. Elife 10, e61276. 10.7554/eLife.61276.